

# Model-free Online Motion Adaptation for Optimal Range and Endurance of Multicopters

Andrea Tagliabue, Xiangyu Wu, and Mark W. Mueller

**Abstract**—In this work we introduce an approach that allows a quadcopter to find the velocity which maximizes its flight time (endurance) or flight distance (range) while moving along a given path, using on-board power measurement. The proposed strategy is based on Extremum Seeking Control and (a) does not require any model of the power consumption of the system, (b) can be executed on-line, and (c) guarantees adaptation to unknown disturbances. We show in experiment that hovering is not the most energy-efficient loitering strategy, and we demonstrate the proposed method’s ability to adapt to different aerodynamic disturbances, such as payloads, while flying at the optimal range velocity along a circular path. The method may be especially useful in applications where a quadcopter carries an unknown payload, allowing it to adapt for improved range.

## I. INTRODUCTION

Multicopters are gaining increasing interest as tool for critical, real-world, outdoor applications such as search and rescue [1], inspection [2] and transportation [3]. Due to the relatively simple and inherently redundant mechanical design, their popularity is also raising for manned transportation [4] and space exploration [5], [6] applications. However, the limited flight time and distance of most of the available platforms [7] severely constraint their range of applications.

A possible solution to limited flight autonomy is the deployment of novel designs, such as Vertical Take Off and Landing (VTOL) platforms [8], [9], tethered multicopters [10] and hybrid solutions [11]. For existing platforms, efficiency can be improved via hardware optimization (e.g. by reducing the weight) or via algorithm-based optimization.

Algorithm-based optimization offers multiple opportunities for the improvement of efficiency of aerial machines, as it is easy to implement, economic to deploy, and can be used to complement mechanical designs, gaining insights for novel hardware platforms. Algorithmic improvements can be achieved via a model-based or a model-free approach. A model-based approach (e.g. [12], [13], [14]) allows to fully exploit the capabilities of the system, but relies on the ability to derive and identify an adequate model of the power consumption of a multicopter. Such a model is usually focused on capturing the electrical power losses [15], [16], [17], or the aerodynamic power losses [18] [19], [20] of the robot. A model-free approach (e.g. [21]), instead, allows to better take into account hard-to-model, less known effects, such as changes in performance due to aging of the components, or changes in the aerodynamic due to payloads.

The authors are with the High Performance Robotics Lab, University of California, Berkeley, CA 94703, USA.  
andrea.tagliabue@me.com, {wuxiangyu, mwm}@berkeley.edu

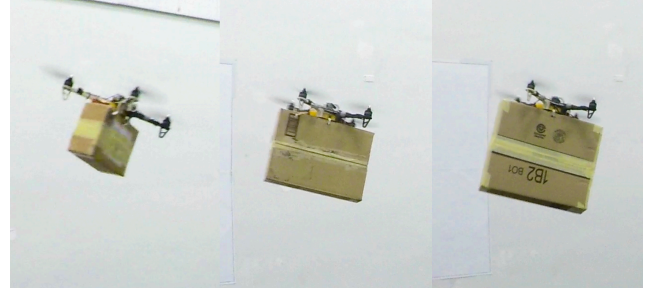


Fig. 1. Quadcopter carrying different payloads with similar mass but different size. The proposed control scheme allows to find the speed that maximizes the flight distance of the vehicle along a given path. It adapts to unknown disturbances, such as the aerodynamic interference from a payload.

In this work we present an on-line, model-free, adaptive approach to find the velocity which maximizes the total flight time (endurance or loitering time) or flight distance (range) of a quadcopter, using Extremum Seeking (ES) control. ES control is peak-finding technique and it is thoroughly described in e.g. [22]. It has found a relatively wide usage in robotics, as detailed in the literature survey [23]. Its applications include aeronautics, where it is employed to increase power efficiency in formation flight [24]. In our work, ES control is used to minimize derived cost functions which express the endurance and range of the robot as a function of its velocity, given a fixed energy budget. The proposed scheme autonomously sets the reference velocity along a predefined path according to the chosen cost function. By flying along a circular path with a quadcopter, we show that the algorithm allows to find the optimal, non-zero, loitering velocity. We demonstrate that our approach successfully adapts the reference velocity to the optimal range velocity in multiple flight scenarios, such as the transportation of the different payloads shown Fig. 1. In addition, we compare our experimental results with the predictions from a derived dynamic model of the power consumption of a quadcopter.

The remainder of this work is organized as follows: Section II describes a model of the power consumption of a quadcopter; Section III introduces the peak-finding scheme based on ES control; Section IV shows experimental results and the identification of the model parameters.

## II. DYNAMIC MODEL OF A QUADCOPTER UAV

In this section we derive the dynamic model of a quadcopter that takes into account the electrical power consumption, as measured at the terminals of the on-board battery. Such a model allows to justify some of the counterintuitive

properties of the system observed in our experimental results (e.g. power consumption is not monotonically increasing w.r.t. velocity), and allows to make predictions on the behavior of the system beyond the capabilities of our experimental testbed.

### A. Reference frame definition

As shown in Fig. 2, we define two sets of coordinate frames: an inertial frame  $I$  and a non-inertial frame  $B$ , attached to the Center of Mass (COM) of the quadcopter.

### B. Quadcopter dynamics

The quadcopter is modeled as a rigid body with six degrees of freedom. Its translational and rotational dynamics are described by the following set of Newton-Euler equations:

$$m\ddot{x} = mg + R \sum f_i + f_d \quad (1)$$

$$\dot{R} = R[\omega] \quad (2)$$

$$I\dot{\omega} = -\omega \times I\omega + \sum \tau_i \quad (3)$$

The vector  $x$  and its derivatives express the vehicle's translational position, velocity and acceleration in the inertial reference frame  $I$ , while  $\omega$  and its derivative define the angular velocity and acceleration in the body-fixed frame  $B$ . Each propeller  $i$  ( $i = 1, \dots, 4$ ), produces a thrust force  $f_i = (0, 0, f_i)$  and a torque  $\tau_i = (0, 0, \tau_i)$ , expressed in  $B$ . We additionally introduce the rotation matrix  $R$ , which relates the body-fixed and world-fixed frames, and the gravity vector  $g = (0, 0, -g)$ , expressed in  $I$ . The vector  $f_d$ , also expressed in  $I$ , represents the drag force modelled as an isotropic drag, which is the sum of a linear and a quadratic term (see e.g. [25]):

$$f_d = -(\mu_1 \nu_\infty + \mu_2 \nu_\infty^2) e_{\nu_\infty} = f_d e_{\nu_\infty} \quad (4)$$

$$e_{\nu_\infty} = \frac{\nu_\infty}{\|\nu_\infty\|}, \quad \text{where } \nu_\infty = \|\nu_\infty\|$$

where  $\nu_\infty$  corresponds to the freestream velocity expressed in  $I$ . The scalars  $\mu_1$  and  $\mu_2$  represent the drag coefficients and can be identified experimentally. We additionally assume that the drag force acts on the COM of the multicopter and thus no torques are produced.

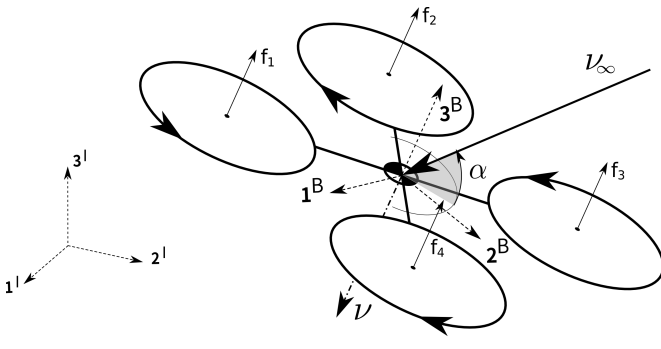


Fig. 2. Coordinate frame definition.  $I$  represents the inertial reference frame and  $B$  the quadcopter reference frame. We additionally show the thrust force of the  $i$ -th propeller  $f_i$ , the freestream velocity  $\nu_\infty$ , the induced velocity  $\nu$  and the angle of attack  $\alpha$ , shown positive in the diagram.

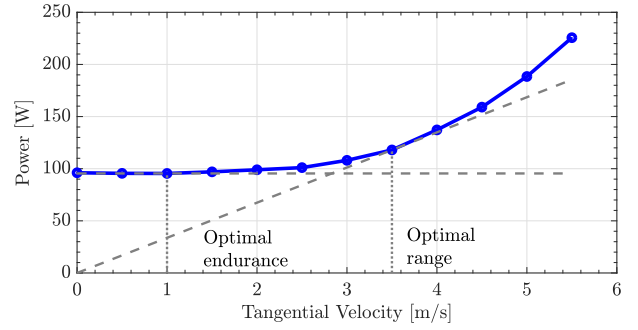


Fig. 3. Power-velocity curve obtained by flying a quadcopter at different velocities along a horizontal circular path of radius  $r = 1.7$  m. We have highlighted the optimal endurance velocity, corresponding to the speed that minimizes the electrical power consumption, and the optimal range velocity, corresponding to the speed that minimizes the ratio between power and velocity. According to the proposed model, the power consumption at optimal endurance velocity further decreases by flying along a straight path.

### C. Power losses

Following [7], [12], [21], we assume that the total power consumption  $p$  (measured at the terminals of the battery) is proportional to the *aerodynamic induced power* [20]  $p_{\text{induced}}$ :

$$p = \frac{1}{\eta} p_{\text{induced}} \quad (5)$$

where  $\eta$  lumps the conversion losses in the energy flow from the battery to the propellers and can be obtained experimentally. Assuming constant altitude and forward flight and given  $f_{\text{thrust}} = f_1 + \dots + f_4$ ,  $p_{\text{induced}}$  is computed as [20]:

$$p_{\text{induced}} = \sum_{i=1}^4 p_{\text{induced},i} = \sum_{i=1}^4 \kappa (\nu + \nu_\infty \sin \alpha) f_i \quad (6)$$

$$= \kappa (\nu + \nu_\infty \sin \alpha) f_{\text{thrust}}$$

where  $\nu$  represents the induced velocity applied by the propeller to the surrounding air. The angle of attack  $\alpha$  is defined as the angle between  $\nu_\infty$  and the plane given by  $1^B$  and  $2^B$ , as represented in Fig. 2. For simplicity we have assumed the angle of attack  $\alpha$ , the induced velocity  $\nu$  and the freestream flow  $\nu_\infty$  to be the same for every propeller, neglecting effects such as changes in freestream velocity due to non-zero angular rates  $\omega$ . The scalar  $\kappa$  is an empirical correction factor, and can be lumped in the conversion efficiency factor  $\eta$ . The induced velocity  $\nu$  is implicitly defined as [20]:

$$\nu = \frac{\nu_h^2}{\sqrt{(\nu_\infty \cos \alpha)^2 + (\nu_\infty \sin \alpha + \nu)^2}}. \quad (7)$$

The induced velocity at hover  $\nu_h$  is obtained from:

$$\nu_h = \sqrt{\frac{mg/4}{2\rho\pi r^2}} \quad (8)$$

where  $\rho$  is the density of the air and  $r$  is the radius of the propellers. Equation (7) can be solved for  $\nu$  using numerical techniques such as the Newton-Raphson [26].

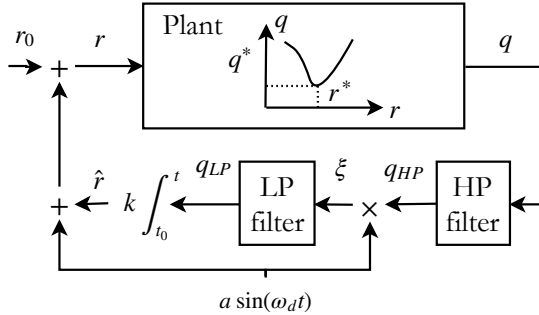


Fig. 4. Block diagram of a feedback scheme based on Extremum Seeking (ES) control. The scalar  $r_0$  represents the plant's initial setpoint. The frequency of the HP and LP filters is set, respectively, to  $\omega_{HP}$  and  $\omega_{LP}$ . The scalar  $k$  is a tuning parameter of the controller: setting  $k > 0$  allows to maximize the output of the plant, while  $k < 0$  minimizes the output.

### III. MODEL-FREE ADAPTIVE CONTROL

In this section we introduce the model-free approach which allows to identify optimal range and endurance velocities of a multicopter, along a predefined reference path. Small changes in the vehicle's velocity can affect the power consumption and thus the autonomy of the vehicle, as illustrated in Fig. 3. Identification via model-based approaches is not always possible, as optimal range and endurance speed depend on multiple electromechanical and aerodynamic properties of the robot, like the thrust to lift ratio of propellers, the drag on the fuselage (e.g. due to payloads), the efficiency of the electric motors and the efficiency of the electronic speed controllers. Unknown or un-modeled disturbances, including wind, aging of the components or payloads, can further affect these optimal operating points. An on-line, adaptive approach seems therefore especially suitable for this task. The proposed scheme based on Extremum Seeking control is detailed in the following paragraphs. A main assumption of this work is that information about the instantaneous power consumption of the vehicle is available, for example by sensing the voltage and current at the battery.

#### A. Extremum Seeking Controller

As shown in Fig. 4, ES control allows to find an unknown, time-varying plant operating point  $r^*(t)$  which maximizes or minimizes a given plant output  $q(t)$ . The optimal setpoint is found by applying a small periodic perturbation  $a \sin(\omega_d t)$  to the current reference setpoint  $\hat{r}(t)$  and by monitoring the changes of the plant's output at the given disturbance frequency  $\omega_d$ . The scalar  $a$  defines the magnitude of the perturbation, while the disturbance frequency  $\omega_d$  is set at a value sufficiently small, so that the plant can be considered a static map. If perturbed plant's input  $r(t) = \hat{r}(t) + a \sin(\omega_d t)$  and output  $q(t)$  are in phase (i.e. input grows, output grows) then the reference setpoint  $\hat{r}(t)$  is decreased (assuming that we are minimizing the cost function). If they are out of phase,  $\hat{r}(t)$ , which corresponds to the current estimate of the optimal operating point, is increased. The persistent nature of the input perturbation  $a \sin(\omega_d t)$  allows to adapt to time-varying systems. A proof of convergence and further details

are provided in [22].

In the context of maximizing the range or endurance of a quadcopter, we employ an ES controller to set the reference tangential speed of the vehicle along a desired path. We define suitable cost functions which relates range (distance flown) and endurance (time flown) to the speed of the vehicle and its instantaneous power consumption. The estimate of the optimal reference tangential velocity, output of the ES controller, is then used to parametrize the desired path into a trajectory, fed as input to the position and attitude controller of the vehicle. A diagram of the system architecture can be found in Fig. 5.

#### B. Cost function derivation

In this section we derive two cost functions, one which relates the velocity of flight of a multicopter with its range distance and one with its endurance time. We assume that it is given a constant energy budget, such as the energy stored in the on-board battery  $E \in [E_{\text{empty}}, E_{\text{full}}]$ . We additionally assume that the vehicle (a) is moving at steady state, with constant ground velocity  $v_{\text{ground}}$ , (b) is using a constant power  $p$ , and (c) is maintaining a constant altitude and orientation along the reference path.

1) *Endurance mode:* The endurance time  $t_{\text{endurance}}$  is defined as:

$$t_{\text{endurance}} := \int_{t_0}^{t_{\text{end}}} dt = \int_{E_{\text{empty}}}^{E_{\text{full}}} \frac{1}{p} dE = \frac{1}{p} \Delta E \quad (9)$$

by considering that  $t_0$  and  $t_{\text{end}}$  represent initial and final time of the mission, corresponding respectively with the full and empty states of the on-board battery  $E_{\text{full}}$  and  $E_{\text{empty}}$ , with  $\Delta E = E_{\text{full}} - E_{\text{empty}}$ . From (9), and given that the total energy in the battery  $\Delta E$  is constant, follows that:

$$\max(t_{\text{endurance}}) \Leftrightarrow \max\left(\frac{1}{p}\right) \Leftrightarrow \min(p) \quad (10)$$

2) *Range mode:* The range distance  $d_{\text{range}}$  is defined as:

$$d_{\text{range}} := \int_{t_0}^{t_{\text{end}}} v_{\text{ground}} dt = \int_{E_{\text{empty}}}^{E_{\text{full}}} \frac{v_{\text{ground}}}{p} dE = \frac{v_{\text{ground}}}{p} \Delta E \quad (11)$$

From (11) follows that:

$$\max(d_{\text{range}}) \Leftrightarrow \max\left(\frac{v_{\text{ground}}}{p}\right) \Leftrightarrow \min\left(\frac{p}{v_{\text{ground}}}\right). \quad (12)$$

3) *Stability and performance considerations:*

a) *Stability:* convergence of the ES control scheme is guaranteed only if the magnitude of the additive disturbance  $a \sin(\omega_d t)$  on the reference velocity is sufficiently small [22], and  $\omega_d$  is sufficiently smaller than the natural frequency of the quadcopter. Tuning of the controller requires then to identify three different time scales in the controlled system: (a) a “fast” time scale, defined by the dominant (slowest) dynamics of the plant. In our case this value is set to the dominant pole of the position controller of the quadcopter; (b) a “medium” time scale, which corresponds to the frequency  $\omega_d$  of the disturbance of the ES controller;

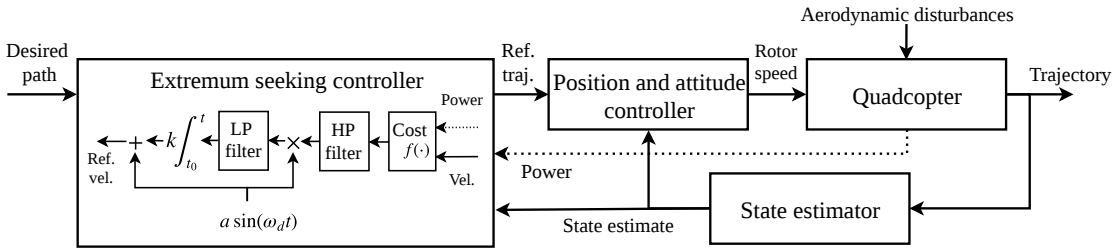


Fig. 5. System diagram employed for on-line optimization of the range or endurance of a quadcopter UAV. Given a desired path, such as a circle of constant altitude and radius, the Extremum Seeking (ES) controller generates a reference trajectory which is tracked by the UAV via the position and attitude controller. The reference trajectory is generated by defining a reference velocity along the desired path. The ES controller automatically sets the reference velocity which minimizes a given cost function  $f(\cdot)$ , according to the information provided by the motion capture system about the estimated velocity of the UAV and the current and voltage measurements from the sensors mounted on-board.



Fig. 6. Hardware used for the experimental results.

(c) a “slow” time scale, which correspond to the dominant frequency of the high-pass and low-pass filters employed in the ES controller.

*b) Performance:* while stability requirements significantly limit the convergence speed of the controller, they imply that the action of the persistent disturbance output by the ES controller has little effect on the worsening of the power consumption, as the accelerations introduced by the periodic perturbation are small. Furthermore, we observe that due to the persistent input perturbation, which guarantees time-varying adaptation, the controller only converges to a neighborhood of the optimal setpoint. Convergence time, in addition, is limited by the speed of the dominant frequency of the plant (for the time scale separation requirement).

#### IV. EVALUATION

In this section we present the experimental results to validate the effectiveness of the proposed on-line, optimal velocity finding approach. The results show that the algorithm is able to find the optimal range and endurance velocities despite unknown disturbances and starting from different initial velocities. In addition, we present how to identify the parameters of the power model proposed in Section II and validate the model.

##### A. Experimental setup

The vehicle used throughout the experimental results is a custom-built quadcopter, shown in Fig. 6, where we also

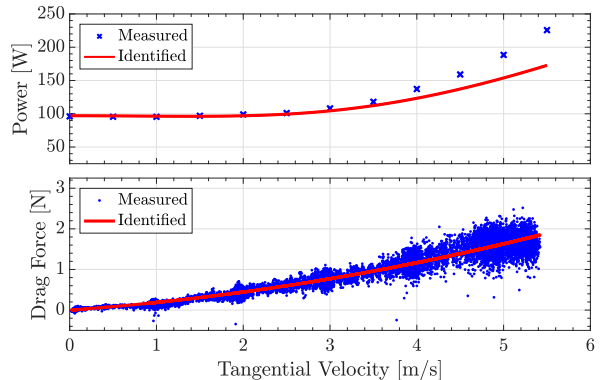


Fig. 7. (Top:) Power-velocity curve measured and predicted by our model. (Bottom) Drag force as a function of the velocity and model prediction with the identified parameters. The identification setup has been obtained by flying a quadcopter without payload along a horizontal circular path of radius  $r = 1.7$  m.

show the payloads used for validation of the proposed approach. The on-board attitude controller runs at 500 Hz on a Bitcraze Crazyflie [27] electronic board with a modified version of the PX4 firmware [28]. Position and other controllers run off-board, sending commands to the vehicle via a radio link at 50 Hz. The experiments are executed indoor, using a commercial motion capture system for the localization of the vehicle. Due to the size of the flight space, we fly along circular paths with a maximum radius of approximately 2.15 m.

##### B. Model identification and validation

In this section we validate the modeling assumptions presented in Section II. We identify the model parameters and compare the predicted and measured power consumption by flying along a horizontal circular trajectory at different velocities. We assume that the efficiency of the powertrain and propellers is lumped in the parameter  $\eta$ , which is identified as:

$$\eta = \frac{\hat{p}_h}{mg\nu_h} \quad (13)$$

where  $\hat{p}_h$  corresponds to the measured electrical power consumption at hover, obtained via the on-board voltage and

current sensor. The induced velocity at hover  $\nu_h$  is computed according to (8). The drag coefficients are identified by flying at different velocities along a circular trajectory with constant altitude and are obtained according to:

$$\hat{f}_{\text{thrust}} = -\frac{m}{\cos \phi \cos \theta} g \quad (14)$$

$$\hat{f}_{\text{drag}} = (\hat{f}_{\text{thrust}} \mathbf{R} \mathbf{3}^I) \cdot \mathbf{e}_{\nu_\infty} - m \dot{\nu}_\infty. \quad (15)$$

where for simplicity and to reduce the effects of noise we have assumed that the vehicle only moves horizontally. The angles  $\phi$  and  $\theta$  correspond, respectively, to the roll and pitch of the vehicle. From the identification experiment, we obtain that the powertrain efficiency  $\eta \approx 0.310$ , the linear drag coefficient  $\mu_1 \approx 0.153 \text{ N m}^{-1} \text{s}$  and the quadratic drag coefficient  $\mu_2 \approx 0.035 \text{ N m}^{-2} \text{s}^2$ . A comparison of the estimated and measured power consumption, as well as the measured and identified drag, is shown in Fig. 7, where we fly along a circular trajectory of radius 1.7 m at high speed. We remark that the validation dataset is different from the one used for identification of the parameters of the model. We can observe that the model predicts the power consumption well up to about  $3.5 \text{ m s}^{-1}$ , and then tends to underestimate the power demand, potentially due to the simple modeling assumption regarding the electrical power losses.

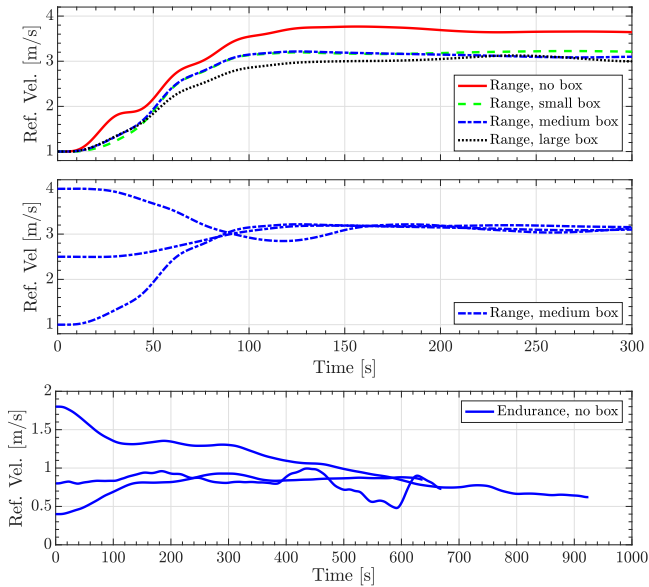


Fig. 8. Experimental results of the convergence of the Extremum Seeking (ES) controller. In the first plot we observe that the optimal range velocity differs due to the aerodynamic properties of the transported payload ( $\approx 3.0 \text{ m s}^{-1}$  for large box,  $\approx 3.1 \text{ m s}^{-1}$  for medium,  $\approx 3.2 \text{ m s}^{-1}$  for small, and  $\approx 3.6 \text{ m s}^{-1}$  with no box). In the second and third plot we observe that optimal range and endurance velocity converge despite the different initial values. The optimal endurance velocity is non-zero due to the effect of the induced power consumption. The changes in power and energy per meter for the different scenarios are represented in Fig. 10 and Fig. 9 respectively.

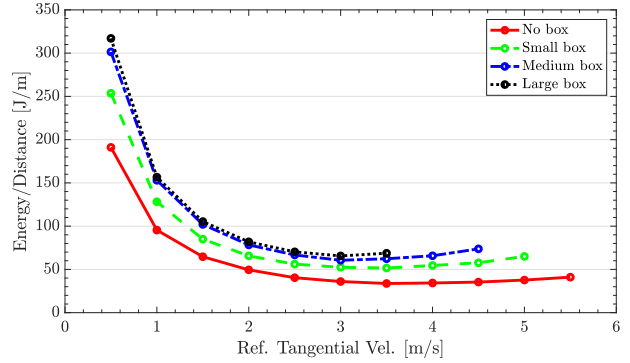


Fig. 9. Cost function, expressed as energy/distance, used by the ES controller to find the optimal range velocity of a quadcopter. The cost function presents a minimum at  $\approx 3.0 \text{ m s}^{-1}$  when a cardboard box is attached to the quadcopter, and a minimum at  $\approx 3.5$  when no payload is attached. These results are in agreement with the convergence velocities shown in Fig. 8 (first and second rows).

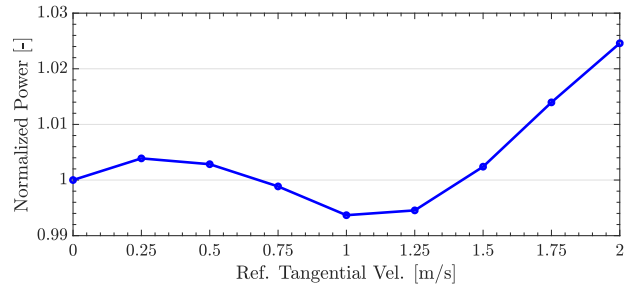


Fig. 10. Normalized power of the vehicle flying at different tangential velocities (with no box), which corresponds to cost function used by the ES controller to find the optimal endurance velocity.

### C. Optimal range and endurance velocities along a circular path

In this part we present the experimental results from the online peak-finding scheme based ES control, which is used to find the optimal range and endurance velocities of a quadcopter flying a circular path. As described in Section III-B.3.a, the magnitude of the reference disturbance  $\omega_d$  is set to  $0.2 \text{ rad s}^{-1}$ , which is about one decade slower than the closed-loop dynamic of the position controller, whose dominant frequency is set to  $2.0 \text{ rad s}^{-1}$ . We empirically found that a good value for the amplitude of the disturbance  $a$  is  $0.15 \text{ m s}^{-1}$ . If faster convergence speed is required and a larger disturbance can be tolerated, the magnitude of disturbance  $a$  can be slightly increased.

1) *Optimal range velocity*: Convergence to optimal range velocities is demonstrated by flying a quadcopter of mass 0.665 kg with different payloads along a horizontal circular path of radius 1.7 m. The employed cost function corresponds to minimize the expression derived in (12), where the power measurement  $p$  is provided by on-board sensors and the velocity  $v_{\text{ground}}$  is obtained from the output of the state estimator. The ES controller is tuned so that the gain  $k$

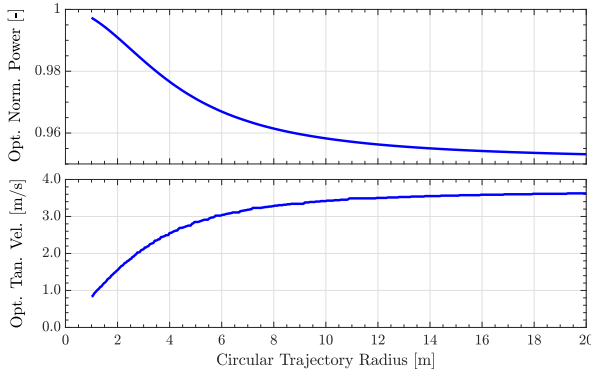


Fig. 11. Optimal endurance velocity and hover-normalized power consumption as a function of the trajectory radius for a quadcopter of mass  $m = 0.695$  kg and identified drag coefficients, estimated according to the proposed lumped model. We can observe that the proposed model predicts a minimum power consumption of approximately 95% of the value at hover for circular paths of radius larger than approx. 10 m.

is set to  $-1$ , and the cutoff frequencies of the HP filter  $\omega_{\text{HP}}$  and LP filter  $\omega_{\text{LP}}$  are set to  $0.1 \text{ rad s}^{-1}$ .

Experiments were executed using different cardboard boxes acting as payloads, and with no payload. The box was oriented so that its largest surface was facing the direction of motion of the vehicle. By varying the size of the box while maintaining approximately the same weight of  $0.2$  kg, we are able to show convergence to different velocities. Fig. 1 shows photographs of the vehicle with the boxes, as used in the experiment.

The experimental results are shown in the first and second rows of Fig. 8, where we display the estimate of the optimal reference tangential velocity, as computed by the ES controller. In order to verify that the reference velocity converges to the optimal value, in a separate experiment we fly for  $60$  s at different tangential velocities, along a circular path of the same radius as before, and we record the value assumed by the employed cost function. The results are shown in Fig. 9.

By comparing the convergence velocities of the ES controller in the first row Fig. 8 with data in Fig. 9, we observe that the proposed method is able to find the optimal range velocities despite the difference in payloads. In addition, the second row of Fig. 8 shows that the method is able to find the optimal range velocity despite starting from different initial velocities.

2) *Optimal endurance velocity:* Similar to the optimal range case, convergence to the optimal endurance velocity is shown by flying along a circular path of radius  $2.15$  m at a fixed altitude, using a quadcopter of  $0.695$  kg and no box attached. The employed cost function corresponds to minimizing the power measured on-board, as derived in (10). The gain  $k$  of the ES controller is set to  $-1$ , while  $\omega_{\text{HP}} = \omega_{\text{LP}} = 0.02 \text{ rad/sec}$ . The convergence results are displayed in the third row of Fig. 8, where we plot the estimate of the optimal reference tangential velocity, output of the ES controller (without sinusoidal disturbance). For

comparison, Fig. 10 represents the value of the employed cost function, obtained by flying for  $20$  s at different tangential velocities along the same circular path. In this case we observe that the minimum of the cost function, which corresponds to a reduction of approximately  $1\%$  of the power at hover, is reached for a non-zero reference tangential velocity, corresponding to about  $1 \text{ m s}^{-1}$ . Such effect is due to the reduction in induced power consumption for increasing freestream velocity, as detailed by [20] and also observed by [7], [12], and justifies why hovering is not the optimal loitering strategy. From Fig. 8 (third row) we can observe that the reference tangential velocity successfully converges to the minimum of the cost function measured in Fig. 10. From the derived model we can additionally observe that increasing the radius of the circular path helps to increase the autonomy of the robot. As shown in Fig. 11, our model predicts an improvement of approx.  $5\%$  of the power consumption at hover for paths with radius larger than  $10$  m.

## V. CONCLUSION AND FUTURE WORKS

In this work we have presented a method to find the velocity which maximizes the flight distance (range) or time (endurance) of a multicopter, given a desired path. Experiments show that the proposed approach is able to converge to the optimal velocity independent of the initial speed of the robot. By varying the aerodynamic drag of the vehicle with different payloads, we additionally show that our method allows to adapt the optimal range velocity to unknown disturbances. From our modeling efforts and experimental results we observed that, for circular paths with sufficiently large radius, the total power consumption as a function of the freestream velocity of the multicopter is not monotonically increasing, but presents a minimum for non-zero velocity. This means that the optimal loitering strategy is not hovering, but rather flying with some velocity along a straight line or along a circular trajectory of sufficiently large radius. Our experiments achieved a repeatable improvement w.r.t. the electrical power consumption at hover (Fig. 10), while flying along a circular path. Our model predicts further improvements as the radius of the path increases (Fig. 11), but we could not verify the consumption along circular paths with larger radius due to the limited space available.

For future work, we plan to improve the convergence rate of the proposed adaptive method. We also plan to experiment with different desired trajectories outdoor to further validate the effectiveness of the method.

## ACKNOWLEDGEMENTS

This work was supported by the Zeno Karl Schindler Foundation (ZKSF) Master Thesis Grant, Swiss Friends of the United States Association (SFUSA) Study Grant and the CHSR Corporation. Andrea Tagliabue thanks Raffaello D'Andrea for his support to the academic exchange. The experimental testbed at the HiPeRLab is the result of contributions of many people, a full list of which can be found at [hiperlab.berkeley.edu/members/](http://hiperlab.berkeley.edu/members/).

## REFERENCES

- [1] R. Bähnemann, D. Schindler, M. Kamel, R. Siegwart, and J. Nieto, "A decentralized multi-agent unmanned aerial system to search, pick up, and relocate objects," *arXiv preprint arXiv:1707.03734*, 2017.
- [2] K. Steich, M. Kamel, P. Beardsley, M. K. Obrist, R. Siegwart, and T. Lachat, "Tree cavity inspection using aerial robots," in *Intelligent Robots and Systems (IROS), 2016 IEEE/RSJ International Conference on*. IEEE, 2016, pp. 4856–4862.
- [3] A. Tagliabue, M. Kamel, S. Verling, R. Siegwart, and J. Nieto, "Collaborative transportation using mavs via passive force control," in *Robotics and Automation (ICRA), 2017 IEEE International Conference on*. IEEE, 2017, pp. 5766–5773.
- [4] "Kitty hawk," <https://kittyhawk.aero/>, (Accessed on 08/27/2018).
- [5] "Shapeshifters from science fiction to science fact: Globetrotting from titan's rugged cliffs to its deep seafloors," [https://www.nasa.gov/directorates/spacetech/niac/2018\\_Phase\\_I\\_Phase\\_II/Shapeshifters\\_from\\_Science\\_Fiction\\_to\\_Science\\_Fact](https://www.nasa.gov/directorates/spacetech/niac/2018_Phase_I_Phase_II/Shapeshifters_from_Science_Fiction_to_Science_Fact), (Accessed on 09/02/2018).
- [6] R. Lorenz *et al.*, "Dragonfly: A rotorcraft lander concept for scientific exploration at titan," *Johns Hopkins APL Technical Digest*, 2018.
- [7] K. Karydis and V. Kumar, "Energetics in robotic flight at small scales," *Interface focus*, vol. 7, no. 1, p. 20160088, 2017.
- [8] S. Verling and J. Zilly, "Modeling and control of a vtol glider," *Bachelor Thesis, Autonomous Systems Lab, ETH Zurich*, 2013.
- [9] "Uber elevate | the future of urban air transport," <https://www.uber.com/info/elevate/>, (Accessed on 08/27/2018).
- [10] S. Lupashin and R. D'Andrea, "Stabilization of a flying vehicle on a taut tether using inertial sensing," in *Intelligent Robots and Systems (IROS), 2013 IEEE/RSJ International Conference on*. IEEE, 2013, pp. 2432–2438.
- [11] A. Kalantari and M. Spenko, "Design and experimental validation of hytaq, a hybrid terrestrial and aerial quadrotor," in *Robotics and Automation (ICRA), 2013 IEEE International Conference on*. IEEE, 2013, pp. 4445–4450.
- [12] J. Ware and N. Roy, "An analysis of wind field estimation and exploitation for quadrotor flight in the urban canopy layer," in *Robotics and Automation (ICRA), 2016 IEEE International Conference on*. IEEE, 2016, pp. 1507–1514.
- [13] N. Bezzo, K. Mohta, C. Nowzari, I. Lee, V. Kumar, and G. Pappas, "Online planning for energy-efficient and disturbance-aware uav operations," in *Intelligent Robots and Systems (IROS), 2016 IEEE/RSJ International Conference on*. IEEE, 2016, pp. 5027–5033.
- [14] F. Morbidi, R. Cano, and D. Lara, "Minimum-energy path generation for a quadrotor uav," in *Robotics and Automation (ICRA), 2016 IEEE International Conference on*. IEEE, 2016, pp. 1492–1498.
- [15] C. Ampatis and E. Papadopoulos, "Parametric design and optimization of multi-rotor aerial vehicles," in *Applications of Mathematics and Informatics in Science and Engineering*. Springer, 2014, pp. 1–25.
- [16] A. Abdilla, A. Richards, and S. Burrow, "Power and endurance modelling of battery-powered rotorcraft," in *Intelligent Robots and Systems (IROS), 2015 IEEE/RSJ International Conference on*. IEEE, 2015, pp. 675–680.
- [17] Y. Mulgaonkar, M. Whitzer, B. Morgan, C. M. Kroninger, A. M. Harrington, and V. Kumar, "Power and weight considerations in small, agile quadrotors," in *Micro-and Nanotechnology Sensors, Systems, and Applications VI*, vol. 9083. International Society for Optics and Photonics, 2014, p. 90831Q.
- [18] H. Huang, G. M. Hoffmann, S. L. Waslander, and C. J. Tomlin, "Aerodynamics and control of autonomous quadrotor helicopters in aggressive maneuvering," in *Robotics and Automation, 2009. ICRA'09. IEEE International Conference on*. IEEE, 2009, pp. 3277–3282.
- [19] Z. Liu, R. Sengupta, and A. Kurzhanskiy, "A power consumption model for multi-rotor small unmanned aircraft systems," in *Unmanned Aircraft Systems (ICUAS), 2017 International Conference on*. IEEE, 2017, pp. 310–315.
- [20] G. J. Leishman, *Principles of helicopter aerodynamics with CD extra*. Cambridge university press, 2006.
- [21] N. Kreciglowa, K. Karydis, and V. Kumar, "Energy efficiency of trajectory generation methods for stop-and-go aerial robot navigation," in *Unmanned Aircraft Systems (ICUAS), 2017 International Conference on*. IEEE, 2017, pp. 656–662.
- [22] M. Krstić and H. Wang, "Design and stability analysis of extremum seeking feedback for general nonlinear systems," in *Proceedings of the 36th Conference on Decision and Control*.
- [23] B. Calli, W. Caarls, P. Jonker, and M. Wisse, "Comparison of extremum seeking control algorithms for robotic applications," in *Intelligent Robots and Systems (IROS), 2012 IEEE/RSJ International Conference on*. IEEE, 2012, pp. 3195–3202.
- [24] P. Binetti, K. B. Ariyur, M. Krstic, and F. Bernelli, "Formation flight optimization using extremum seeking feedback," *Journal of Guidance, Control, and Dynamics*, vol. 26, no. 1, pp. 132–142, 2003.
- [25] M. Schulz, F. Augugliaro, R. Ritz, and R. D'Andrea, "High-speed, steady flight with a quadrocopter in a confined environment using a tether," in *Intelligent Robots and Systems (IROS), 2015 IEEE/RSJ International Conference on*. IEEE, 2015, pp. 1279–1284.
- [26] J. H. Mathews, *Numerical methods for mathematics, science and engineering*. Prentice-Hall, 1992.
- [27] "Crazyflie 2.0 | bitcraze," <https://www.bitcraze.io/crazyflie-2/>, (Accessed on 05/26/2018).
- [28] L. Meier, P. Tanskanen, L. Heng, G. H. Lee, F. Fraundorfer, and M. Pollefeys, "Pixhawk: A micro aerial vehicle design for autonomous flight using onboard computer vision," *Autonomous Robots*, vol. 33, no. 1-2, pp. 21–39, 2012.